



Source apportionment of black carbon aerosols from light absorption observation and source-oriented modeling: An implication in a coastal city in China

Junjun Deng¹, Hao Guo², Hongliang Zhang³, Jialei Zhu¹, Xin Wang¹, Pingqing Fu¹

5 ¹ Institute of Surface-Earth System Science, School of Earth System Science, Tianjin University, Tianjin 300072, China

² Department of Earth System Science, University of California Irvine, CA 92697-3100, USA

³ Department of Environmental Science and Engineering, Fudan University, Shanghai 200438, China

Correspondence to: Junjun Deng (dengjunjun@tju.edu.cn), Hongliang Zhang (zhanghl@fudan.edu.cn)

Abstract. Black carbon (BC) is the most important light absorbing aerosol in the atmosphere. However, sources of atmospheric BC aerosols are largely uncertain, making it difficult to assess its influence on radiative forcing and climate change. In this study, year-round light-absorption observations were conducted during 2014 using an aethalometer in Xiamen, a coastal city in southeast China. Source apportionment of BC was performed and temporal variations in BC sources were characterized based on both light absorption measurements and a source-oriented air quality model. The annual average concentrations of BC from fossil fuel (BC_{ff}) and biomass burning (BC_{bb}) were $2932 \pm 1444 \text{ ng m}^{-3}$ and $1340 \pm 542 \text{ ng m}^{-3}$, contributing 66.7 % and 33.3 % to total BC, respectively. BC_{bb} contribution exhibited clear diurnal cycle with the highest level (37.9 %) in the evening rush hour and seasonal pattern with the maximum (39.9 %) in winter. Conditional probability function (CPF) analysis revealed the large biomass burning contributions were accompanied by east-northeasterly and northerly winds. Backward trajectory indicated that air masses from north and east-central China were associated with larger biomass burning contributions. Potential source contribution function (PSCF) and concentration-weighted trajectory (CWT) suggested that north and east-central China and Southeast Asia were potential sources for both BC_{ff} and BC_{bb}. The source-oriented modeling results showed that transportation, residential and open biomass burning accounting for 45.3 %, 30.1 % and 17.6 % were the major BC sources. Among the three fuel catalogs, liquid fossil fuel (46.5 %) was the largest source, followed by biomass burning (32.6 %) and coal combustion (20.9 %). Source contributions of biomass burning and fossil fuel combustion identified by the source-oriented model and observation-based method were in good agreement. The source-oriented model also captured the majority of seasonal variations in source contributions. The findings provide solid supports for controlling fossil fuel sources to limit the impacts of BC on climate change and environmental degradation in the relatively clean region in China.

10
15
20
25



1 Introduction

Black carbon (BC) aerosol is a vital air pollutant throughout the surface earth system and it has attracted a great concern regarding its multiple impacts on human health, climate change and atmospheric visibility (Bond et al., 2013). As the most important light-absorbing component of $PM_{2.5}$ (particulate matters with aerodynamic diameter less than $2.5 \mu m$), BC exerts a key and unique role in the climate system by absorbing solar radiation, affecting chemical/physical properties of cloud, and influencing snow and ice cover (Jacobson, 2002; Ramanathan and Carmichael, 2008; Bond et al., 2013; Qian et al., 2014; Kim et al., 2015). BC is even found as the second most important climate-warming agent after carbon dioxide, with a positive climate forcing of $1.1 W m^{-2}$, greater than that of methane (Bond et al., 2013). BC also has impacts on urban weather conditions and may play a key role in extreme weather (Ding et al., 2013; Fan et al., 2015; Saide et al., 2015; Wang et al., 2018). Under polluted environments, BC has significant influence on pollution development (Ding et al., 2016; Peng et al., 2016; Lou et al., 2019). In addition, BC leads to visibility impairment because of its strong absorption of visible light (Watson, 2002) and has adverse impacts on human health due to its adsorption captivity (Janssen et al., 2011; Colicino et al., 2017). Nevertheless, due to lacking observational constraints and uncertainties in emission inventories, large uncertainties still exist in BC emissions including absolute fluxes and relative source contributions of fossil versus biomass combustion, which will complicate our knowledge on the multiple BC effects. It is also necessary to clarify the contributions of different sources to BC in order to determine efficient emission mitigation strategies. At global scale, BC emission sources can be attributed to fossil fuels ($\sim 40 \%$), open biomass burning ($\sim 40 \%$) and biofuels ($\sim 20 \%$) (Ramanathan and Carmichael, 2008). However, these fractions vary significantly because of the substantial spatial and temporal variations in BC emissions (Venkataraman et al., 2005; Rehman et al., 2011; Cheng et al., 2013; Andersson et al., 2015).

Several source apportionments for quantitatively differentiating between biomass and fossil sources of ambient BC aerosol have been conducted using observation-based methods, such as isotope (e.g., radiocarbon) analysis technique and light-absorbing property analysis (Sandradewi et al., 2008; Gustafsson et al., 2009; Liu et al., 2014; Vaishya et al., 2017; Helin et al., 2018; Kalogridis et al., 2018; Mousavi et al., 2018; Jing et al., 2019; Kant et al., 2020). For example, Andersson et al. (2015) presented dual carbon isotope constrained BC source apportionment in three key hotspot regions in China during a severe haze event, finding that biomass burning contributed $\sim 30 \%$ to BC whereas fossil fuel sources were dramatically different between north and south. Aethalometer model was adopted to analyze light absorption at multi-wavelengths to assess the fossil fuel and biomass combustions contributions to BC in Delhi, revealing that the contribution of biomass burning was 28% in average (Dumka et al., 2018). Mousavi et al. (2019) apportioned BC in the Milan metropolitan area to the fossil fuel and biomass burning emission using the Aethalometer model with the absorption Ångstrom exponent (AAE) values derived from the ^{14}C radiocarbon analysis, highlighting the significant impact of residential wood burning on BC. Such observation-based source apportionment methods are powerful to understand the BC



sources at given receptor locations. However, the methods are highly dependent on accurate observations with high temporal
60 resolution, which is unavailable for most regions without the measurement instruments. For example, the isotope method,
especially the ^{14}C analysis, is costly and lack of high temporal resolution. Therefore, although many observation-based BC
source apportionments have been carried out, the source-based method can still be a strong supplement. For example, in a
recent report, Winiger et al. (2019) conducted observation-based source apportionment of circum-Arctic BC with carbon
isotope analysis and found that comparison of a Lagrangian atmospheric transport model (FLEXPART-ECLIPSE-GFED)
65 predictions with the observations agreed well with each other for BC concentrations, with larger discrepancies for
(fossil/biomass burning) sources, indicating the misallocations of emissions in the emission inventories.

Source-oriented modeling, which estimates pollution levels and identifies sources using chemical transport models (CTMs)
with the inputs of emission inventory and meteorology, is another useful tool to study potential factors deriving BC. Such
source apportionment technique has been developed and used for direct source apportionment of PM in more than a decade
70 (Kleeman et al., 2007; Ying et al., 2008; Zhang et al., 2014). For example, Hu et al. (2015) found that residential emission
was the major contributor to BC in spring and winter while industrial emission was important in summer and fall in China.
Guo et al. (2017) quantified the contributions of different sources in North India and found that industry was the largest
source for BC. Although the source-oriented modeling is powerful, limitations exist such as the inability to take into account
unknown sources and the imprecise information on emission inventories and meteorology. The method is highly dependent
75 on accuracy of emission inventory, which is unfortunately an enormous challenge. A pollution source not in the emission
inventory will not emerge as a contributor to the CTM results. Taking into account the advantages and disadvantages of the
observation- and modeling-based methods, a combination of the two methods can be a complement to each other for
providing reliable and reasonable information on pollution sources and contributions.

China is the largest source of BC aerosols in the world (Wang et al., 2012; Bond et al., 2013; Huang et al., 2016), remarkable
80 influences of BC on air quality, weather condition and climate change were revealed in China (Menon et al., 2002; Ding et
al., 2016; Huang et al., 2016; Yang et al., 2017). Spatiotemporal distributions and regional transport mechanisms of BC in
China as well as their affecting factors have been widely investigated with field measurements or model simulations (Cao et
al., 2010; Wu et al., 2013; Wang et al., 2015; Zhang et al., 2019; Zheng et al., 2019; Deng et al., 2020). In contrast, source
apportionment studies on BC aerosols in China are still limited and mostly distributed in heavily polluted areas (Chen et al.,
85 2013; Andersson et al., 2015; Li, K. et al., 2016; Li, N. et al., 2016; Yu et al., 2018; Jing et al., 2019). In this study, the
observation-based method was combined with the source-oriented modeling to quantify the contributions of different sources
to BC in a relatively clean region in China. The results of the two source apportionment methods were inter-compared.
Temporal variability, potential sources and transport pathways of BC from fossil fuel and biomass burning were also
characterized. The findings help better understand main sources and relative contributions of BC and provide valuable
90 information to adopt effective emission reduction measures to control BC pollution in not heavily polluted regions.



2 Methodologies

2.1 Observation site and measurements

The field campaign was performed in Institute of Urban Environment, Chinese Academy of Sciences (118°03'E, 24°36'N) in the coastal city Xiamen in China (Deng et al., 2016, 2020). Xiamen is located in the Western Taiwan Strait region, which is adjacent to the Yangtze River Delta region (YRD) and the Pearl River Delta region (PRD) (Fig. 1). Xiamen has small local emission of BC (Fig. 1) and better diffusion condition compared to some developed cities in East China, which might lead to a lower BC concentration in Xiamen (Deng et al., 2020). However, Xiamen is often affected by emissions from polluted areas by long-range transport under the influence of East Asia monsoon (Deng et al., 2020). Therefore, conducting source apportionment of BC over Xiamen is very representative to improve our understanding on the sources of BC and their transport characteristics in relatively clean region.

The observation site lies approximately 15 km away from the downtown to the southeast. None of large industrial sources was within 10 km away and there were only a few construction and traffic sources. The measurement instruments were arranged on the rooftop of a house with a height of 8 m above ground level. Real-time measurements of BC mass concentration were conducted with a seven-wavelength (370, 470, 520, 590, 660, 880 and 950 nm) aethalometer (AE31, Magee Scientific) in January–December 2014. Aethalometer worked at a flow rate of 5 L min⁻¹ and estimated light attenuation under the principle of optical transmission (Hansen et al., 1984). BC concentration was then calculated according to the light attenuation. The concentration measured at 880 nm is considered as the standard value of atmospheric BC because BC is the predominant light-absorbing species at this wavelength with little impact from other compounds (Ganguly et al., 2005). The method reported in Virkkula et al. (2007) was applied to correct BC mass concentration due to shadowing effects and multiple scattering effects.

2.2 Observation-based source apportionment

Observation-based source apportionment of BC in Xiamen was performed with the Aethalometer method, which is based on the two-component assumption and has been widely adopted to assess the contribution from fossil fuel combustion and biomass burning (Sandradewi et al., 2008; Favez et al., 2010; Liu et al., 2014; Rajesh and Ramachandran, 2017; Martinsson et al., 2017; Dumka et al., 2018; Helin et al., 2018; Mousavi et al., 2019; Mbengue et al., 2020). The Aethalometer method apportions the total BC to BC_{ff} (BC emitted by fossil fuels) and BC_{bb} (BC emitted by biomass burning) contributions. BC_{ff} and BC_{bb} are expressed as follows:

$$BC_{ff} = BC \times \frac{b_{abs,ff}(\lambda)}{b_{abs}(\lambda)} \quad (1)$$



$$BC_{bb} = BC \times \frac{b_{abs,bb}(\lambda)}{b_{abs}(\lambda)} \quad (2)$$

120 where $b_{abs}(\lambda)$ is light absorption at wavelength of λ , $b_{abs,ff}$ and $b_{abs,bb}$ are light absorption coefficients for fossil fuel and biomass burning, respectively. b_{abs} is assumed to apporition to $b_{abs,ff}$ and $b_{abs,bb}$ contributions (Sandradewi et al., 2008). $b_{abs,ff}$ and $b_{abs,bb}$ satisfy the following equations:

$$\frac{b_{abs,ff}(\lambda_1)}{b_{abs,ff}(\lambda_2)} = \left(\frac{\lambda_1}{\lambda_2} \right)^{-AAE_{ff}} \quad (3)$$

$$\frac{b_{abs,bb}(\lambda_1)}{b_{abs,bb}(\lambda_2)} = \left(\frac{\lambda_1}{\lambda_2} \right)^{-AAE_{bb}} \quad (4)$$

125 where AAE_{ff} and AAE_{bb} are the absorption Ångström exponents (AAE) for fossil fuel and biomass burning, respectively. AAE_{ff} adopted in present study is 1 since fossil fuel combustions mostly contain BC and typically no other light absorbing constituents (Kirchstetter et al., 2004; Bond et al., 2013). By contrast, in addition to BC, emissions from biomass burning contain a substantial fraction of light absorbing organic aerosols, which strongly enhances light absorption in the near-ultraviolet spectrum and has little contribution in the near-infrared spectrum. Therefore, AAE_{bb} is larger than AAE_{ff} due
130 to the strong absorption in the UV regime (Sandradewi et al., 2008; Bond et al., 2013; Zotter et al., 2017). The empirical value of AAE_{bb} adopted in this work is 2 according to Sandradewi et al. (2008). BC_{ff} and BC_{bb} can be obtained by combining all above equations and assumed values for AAE_{ff} and AAE_{bb} .

In Eqs. (3)–(4), λ_1 and λ_2 should be wavelengths in the near-ultraviolet and near-infrared range, respectively. In this study, 470 nm and 950 nm were selected as near-ultraviolet and near-infrared wavelengths based on previous studies (Sandradewi
135 et al., 2008; Favez et al., 2010; Zotter et al., 2017; Kalogridis et al., 2018).

2.3 Potential sources of BC_{ff} and BC_{bb}

The conditional probability function (CPF) was used to investigate the possible predominant directions of local sources of BC_{ff} and BC_{bb} relative to wind directions in different seasons (Ashbaugh et al., 1985). The CPF is calculated as:

$$CPF_{\Delta\theta} = m_{\Delta\theta} / n_{\Delta\theta} \quad (5)$$

140 where $n_{\Delta\theta}$ is the total occurrences from wind sector $\Delta\theta$ and $m_{\Delta\theta}$ is occurrences from the same wind sector with the BC_{ff} (BC_{bb}) concentration exceeding the threshold criterion. The CPF analysis was also performed for the ratio of BC_{bb} to BC (BC_{bb}/BC) to analyze the impact of local sources on the contribution from biomass burning. In this analysis, a threshold criterion of the top 25 % concentration (ratio) was chosen.

Backward trajectories were simulated with the Hybrid Single Particle Lagrangian Integrated Trajectory model (HYSPLIT)
145 from NOAA/ARL to characterize the regional sources and transport of air masses arriving in Xiamen (Stein et al., 2015).



Five-day backward trajectories ended at the height of 500 m were calculated every hour using the Global Data Assimilation System (GDAS) reanalysis meteorological dataset with a $1^\circ \times 1^\circ$ latitude-longitude resolution. Hourly trajectory endpoints implying the geographical distribution and the height of the air parcel were derived from the model and trajectory clusters were then obtained from cluster analysis. The outflow regimes for air masses to the receptor site with the potential origins were traced with the trajectory clusters.

Potential regional source contributions of BC_{fr} and BC_{bb} were further identified with the potential source contribution function (PSCF) method on basis of the backward trajectories. PSCF is a widely adopted tool to identify regional source distributions of air pollutants at a receptor site (Hopke et al., 1995; Bari et al., 2015; Zhang et al., 2017). The study domain is divided into $i \times j$ grid cells and PSCF values can be calculated as follows:

$$PSCF_{i,j} = m_{i,j} / n_{i,j} \quad (6)$$

where $n_{i,j}$ is the number of endpoints that in the ij th grid cell and $m_{i,j}$ is the number of endpoints for the same grid cell that have BC_{fr} (BC_{bb}) concentration higher than a criterion. These grid cells with high PSCF values are the maximum probability potential source areas contributing to high BC_{fr} (BC_{bb}) mass concentrations at the receptor location. In this work, the top 25 % concentrations were set as the threshold. The study domain covered 10° – 55° N and 80° – 140° E, which composes 10800 grid cells with the size of $0.5^\circ \times 0.5^\circ$ latitude and longitude.

To minimize the uncertainty in grid cells with low $n_{i,j}$, an empirical weight function $w_{i,j}$ was multiplied with the PSCF values. $w_{i,j}$ was defined as follows:

$$w_{i,j} = \left\{ \begin{array}{ll} 1.00 & n_{i,j} > 3n_{ave} \\ 0.70 & 1.5n_{ave} < n_{i,j} \leq 3n_{ave} \\ 0.42 & n_{ave} < n_{i,j} \leq 1.5n_{ave} \\ 0.05 & n_{i,j} \leq n_{ave} \end{array} \right\} \quad (7)$$

It is difficult for PSCF method to identify the source intensity and separate strong sources and weak sources. Therefore, concentration-weighted trajectory (CWT) model was also performed to overcome this limitation. In this method, each grid cell is assigned a weighted concentration by averaging the sample concentrations that have associated trajectories crossing the grid cell (Hsu et al., 2003). The average weighted concentration $C_{i,j}$ in the ij th grid cell was calculated as follows:

$$C_{i,j} = \frac{1}{\sum_{l=1}^M \tau_{i,j,l}} \sum_{l=1}^M C_l \tau_{i,j,l} \quad (8)$$

where M is the total number of trajectories, C_l is the observed BC_{fr} (BC_{bb}) concentration at receptor site on arrival of trajectory l and $\tau_{i,j,l}$ is the number of endpoints in the ij th grid cell of trajectory l . In general, the grid cells with high CWT values are high strength sources. The weighting function $w_{i,j}$ was also adopted in the CWT analysis to reduce the effect of the small values of $n_{i,j}$.



2.4 Source-oriented modeling

In this analysis, source apportionment of BC over Xiamen using an updated source-oriented CMAQ model for primary
175 particulate matter (CMAQ-PPM) (Hu et al., 2015; Guo et al., 2017) was also implemented in addition to the
observation-based source apportionment. The CMAQ-PPM model was updated on basis of CMAQ v5.0.1, which was
developed by the U.S. EPA Atmospheric Science Modeling Division. The photochemical mechanism and aerosol chemistry
mechanism adopted in this study were SAPRC-11 and AERO6, respectively. In the source-oriented model, tagged
non-reactive PM tracers are used to estimate the source contributions of PPM and its chemical components. The PM tracers
180 are set to undergo the same atmospheric processes as other species. The emissions of the tracers are set to 0.001 % of the
PPM emissions from each corresponding source sector and region. It ensures that the tracers will not significantly change the
particle mass and size. After scaling up by 10^5 , the simulated tracer concentration represents the PPM concentrations from a
specific source type/region. The concentrations of the inert chemical components in PPM can be estimated with source
specific emission profiles as follows:

$$185 \quad C_{i,j} = A_{i,j} \times PPM_i \quad (9)$$

where $C_{i,j}$ is the concentration of the j th component from the i th source, $A_{i,j}$ is the ratio of the j th component in PPM mass
from the i th source and PPM_i is the simulated concentration for the i th source. Detailed descriptions of the model can be
found in Hu et al. (2015).

Regional distributions of BC from different categories (sectors) as well as the source category (sector) contributions to BC at
190 the receptor site were determined with the source-oriented CMAQ-PPM model. A 36 km horizontal resolution domain that
covers China and surrounding countries in East Asia (Fig. 1) was applied. There are 18 vertical layers with surface layer
thickness of 35 m and the overall model height of 20 km. The Weather Research & Forecasting model (WRF) v3.9.1 was
utilized to generate meteorology inputs with initial and lateral boundary conditions from NCEP FNL reanalysis data from
NCAR, which is available on $1^\circ \times 1^\circ$ grids continuously for every 6 h (<http://dss.ucar.edu/datasets/ds083.2/>). There are 29
195 vertical layers in the WRF domain. The first eight layers of the WRF and CMAQ domains are identical. The outputs of WRF
were post-processed by Meteorology-Chemistry Interface Processor (MCIP) v4.2 to the format CMAQ requires.
Anthropogenic emissions in China were generated according to the Multi-resolution Emission Inventory for China (MEIC)
developed by Tsinghua University (<http://www.meicmodel.org>). Emissions from other countries and regions outside China
were generated with the Regional emission inventory in Asia version 2 (REAS2) (Kurokawa et al., 2013). The fire emissions
200 were derived from the Fire Inventory from NCAR (FINN) based on satellite observations (Wiedinmyer et al., 2011).
Anthropogenic emissions were grouped into four sectors including industrial, power, transportation and residential. Open
burning emissions are considered as the fifth emission sector. Sources from five sectors were further classified into three
categories such as solid fossil fuel (i.e. coal) combustion, liquid fossil fuel combustion and biomass burning on basis of the



energy consumption data provided by Wang et al. (2012). Spatial distribution of BC concentration over China are depicted in
205 Fig. S1, suggesting that BC concentration in the Western Taiwan Strait region was much lower than that in other urban
agglomerations in north China, east-central China and Sichuan Basin. However, Xiamen was with relatively higher
abundance compared to surrounding areas.

3 Results and discussion

3.1 Light absorption-based source apportionment of BC

210 Fig. 2 demonstrates the temporal variations in daily mean concentrations of BC_{ff} and BC_{bb} with the BC_{bb}/BC fraction in
Xiamen during the field campaign. The missing data were due to the instrument maintenance. Daily concentrations of BC_{ff}
and BC_{bb} were 445 – 9545 $ng\ m^{-3}$ (average: $2932 \pm 1444\ ng\ m^{-3}$) and 334–4031 $ng\ m^{-3}$ ($1340 \pm 542\ ng\ m^{-3}$), respectively.
Daily contribution of BC_{bb} to total BC varied significantly in the range of 18.4 % – 58.3 %. The annual average contribution
of BC_{bb} to BC was 33.3 %, much smaller than that of BC_{ff} (66.7 %), indicating the predominant contribution of fossil fuel
215 combustion in Xiamen. Source apportionment results under different pollution levels of BC and $PM_{2.5}$ in each season were
further investigated to understand BC sources on pollution and clean days (Fig. S2). The data of $PM_{2.5}$ concentration were
from Xiamen Environmental Monitoring Central Station. High (low)-BC periods were the days with the average
concentration of BC higher (lower) than the seasonal average concentration plus (minus) one standard deviation, and so did
 $PM_{2.5}$. Generally, source contributions of BC show obvious variability among different pollution levels in all seasons, and the
220 BC_{bb} percentage decreases with the increasing concentrations of BC and $PM_{2.5}$. Biomass burning contributed more during
low-BC (30.8 % – 43.1 %) and low- $PM_{2.5}$ days (31.5 % – 40.7 %) compared to high-BC (24.8 % – 34.4 %) and high- $PM_{2.5}$
episodes (26.6 % – 36.1 %), implying that emissions from coal combustion and vehicle exhausts are major contributors of
particulate pollution in Xiamen. The fractional contribution of fossil fuel to BC in Xiamen derived by the Aethalometer
method in this work suggests a slighter larger role of fossil fuel compared to that (61 %) estimated according to the
225 “bottom-up” emission inventories (Chen et al., 2013). However, it was similar to the contribution (~ 70 %) in YRD and PRD,
which was estimated based on dual carbon isotope constrained source apportionment (Andersson et al., 2015). BC_{ff} and BC_{bb}
percentages in different regions calculated with the Aethalometer method were summarized in Table S1 for comparison.
 BC_{bb} fraction in Xiamen were overall larger than that in Nanjing in China and other sites in India, suggesting that
contribution of biomass burning increases over the relatively clean region due to the weak emissions of traffic and coal
230 combustion.

Fig. 3 illustrates the diurnal and monthly cycles of BC_{ff} and BC_{bb} concentrations as well as the relative contribution of
biomass burning (BC_{bb}/BC) during the measurements. BC_{ff} exhibited a pronounced diurnal variation, increasing steadily
before dawn with the major morning peak ($4427\ ng\ m^{-3}$) observed around 6:00 in the morning. The high BC_{ff} concentrations



at the observation site from late night to the early morning (~ 21:00 to 8:00) may ascribe to enhanced traffic emissions from
235 diesel trucks during nighttime and cars during rush hours. The heavy diesel trucks, which are major emission sources of BC_{fr} ,
were allowed to enter the city from 22:00 to 7:00. Therefore, BC_{fr} decreased during daytime and reached the diurnal
minimum of 1950 ng m^{-3} at 13:00 in the afternoon. BC_{bb} exhibited a diurnal trend that was different with BC_{fr} . The morning
peak (1755 ng m^{-3}) at 6:00 was also found for BC_{bb} . However, BC_{bb} concentration kept a steady state rather than increase
after 20:00 since BC_{bb} was less influenced by traffic-related emission. Clear diurnal variation in contribution of BC_{bb} to total
240 BC was found. The BC_{bb} fraction reached its valley of 30.4 % at 8:00, increased due to the decrease in traffic emission and
maximized with the ratio of 37.9 % at 19:00 during the rush hour in the evening. The diurnal cycles of BC_{fr} and BC_{bb} were
affected by not only the BC emission trend but also the evolution of atmospheric boundary layer. According to our previous
study on atmospheric boundary layer height in Xiamen (Deng et al., 2020), the boundary layer height was ~three times larger
in the afternoon than that in the early morning, leading to the better diffusion conditions in the afternoon.

245 Monthly mean BC_{bb} concentration peaked with value of 1979 ng m^{-3} in December and reached its valley of 923 ng m^{-3} in
June. The monthly pattern of BC_{fr} was similar but a bit different with that of BC_{bb} . The maximum monthly mean BC_{fr}
concentration was 3636 ng m^{-3} in March, while the minimum was 1881 ng m^{-3} in February. The valley of BC_{fr} concentration
occurring in February was maybe because of the lack of vehicle (e.g., diesel trucks) emissions around the Spring Festival
holiday, which again prove the conjecture in the diurnal pattern of BC_{fr} . Similar to the seasonal pattern of absorption
250 Ångstrom exponent (Qiu et al., 2019), noticeable seasonal variation in the BC_{bb}/BC fraction was found. Winter
(December–February) had the largest BC_{bb} contribution (39.9 %), followed by fall (September–November) (32.1 %), spring
(March–May) (31.1 %) and summer (June–August) (29.6 %). The much larger contribution in winter are possibly due to the
enhanced source from open-field biomass and domestic burning in China. The higher BC_{bb} concentration and contribution
lasted from fall to early winter, consistent with previous emission inventory of biomass burning, which found higher BC
255 emissions from November to February than other months (He et al., 2011). Unlike BC_{fr} , BC_{bb} exhibited an increase trend in
July, leading to a relatively large contribution of BC_{bb} . It might be affected by the long-range transport of air pollutants
emitted from biomass burning in Southeast Asia under the control of summer monsoon (Qiu et al., 2019). The monthly
variation in boundary layer height, which was larger in warm season and smaller in cold season, also affected the monthly
patterns of BC_{fr} and BC_{bb} (Deng et al., 2020).

260 3.2 Sources and transport pathways of BC_{fr} and BC_{bb}

The CPF results for the top 25 % thresholds of concentrations of BC_{fr} (3797 ng m^{-3}) and BC_{bb} (1813 ng m^{-3}) as well as BC_{bb}
contribution (45 %) over different periods are shown in Fig. 4. In the whole year, high BC_{fr} concentrations were mainly
associated with winds from west-southwest to north-northeast with wind speed (ws) $< 2 \text{ m s}^{-1}$ (Fig. 4a). Particularly, high



265 BC_{fr} concentrations were most remarkably distributed in winds from the northwest at low ws ($< \sim 1 \text{ m s}^{-1}$) and to a lesser extent from the west and north-northeast at moderate ws ($< 3 \text{ m s}^{-1}$). It implies the impacts of local sources such as the traffic emissions to the northwest of the site within a short distance. The CPF pattern for BC_{bb} was similar to but not the same with that of BC_{fr} (Fig. 4b). In addition to northwesterly wind with low ws , northeasterly and easterly winds with $ws < 5 \text{ m s}^{-1}$ were also accompanied by high BC_{bb} concentration. Correspondingly, the CPF plot for BC_{bb}/BC fraction implies the significant influence of east-northeasterly wind with $ws > 2 \text{ m s}^{-1}$ on large contribution of biomass burning (Fig. 4c). In addition, northerly wind with wind speed $> \sim 4 \text{ m s}^{-1}$ were also frequently associated with large BC_{bb} fraction. CPF patterns presented obvious seasonality. For BC_{fr} and BC_{bb} , the CPF distributions over spring, summer and fall were similar and the high concentrations were mainly associated with northwesterly wind with $ws < 2 \text{ m s}^{-1}$. However, in winter, additionally with wind from northwest, high BC_{fr} and BC_{bb} concentrations were also frequently associated with wind from southwest and west with $ws < 3 \text{ m s}^{-1}$. For BC_{bb}/BC fraction, large fractions were mainly distributed in northeasterly wind with $ws > 4 \text{ m s}^{-1}$ and most remarkably distributed in winds from the northeast at high ws ($> 6 \text{ m s}^{-1}$) in spring and summer. In fall, east-northeasterly wind with $ws > 3 \text{ m s}^{-1}$ was more frequently associated with large contribution of biomass burning. However, in winter, northerly wind with $ws > 4 \text{ m s}^{-1}$ and northeasterly wind with $ws > 2 \text{ m s}^{-1}$ were most remarkably associated with large BC_{bb} percentage.

Seasonal clusters of backward trajectories obtained by the HYSPLIT model with the average BC_{bb} contributions are illustrated in Fig. 5. Mean concentrations of BC_{fr} , BC_{bb} and BC of each cluster in different seasons are summarized in Table S2. It is clearly shown that originations and transport pathways of air masses arriving in Xiamen exhibited distinct seasonal variations. In summer, air masses were characterized by a predominance of southerly origination. In contrast, in other seasons, air masses from the north had a dominant position, which was particularly the case in winter. Generally, air masses from the northern inland region such as north China and east-central China had larger biomass burning contributions comparing to those from the seas such as East China Sea and South China Sea, since there are dense emissions of biomass burning in northern and eastern China including Hebei, Henan, Shandong and Jiangsu (Huang et al., 2012; Wu et al., 2018). In spring, the eastern cluster (C4) originating from the East China Sea had the lowest BC_{bb} fraction (31 %). However, the northern cluster (C3) originating from Siberia and passing through Mongolia and north and east China had much larger biomass burning contribution (42 %) in comparison to the other clusters. In summer, northeastern coastal cluster (C4) originating from the East China Sea and passing along with East China Coast region had larger biomass burning contribution (38 %). The north cluster passing through Jiangsu, Zhejiang and north Fujian province also had relatively higher BC_{bb} fraction (35 %). In fall, the northern inland cluster (C3) originating from Siberia and passing through the heavily polluted areas such as North China Plain and YRD were associated the largest biomass burning contribution (40 %), followed by the other long-range inland cluster (C2) with the BC_{bb} fraction of 36 %. In winter, similar to spring and fall, the northern cluster from Siberia (C2) had the largest biomass burning contribution (48 %). Contrarily, the northeastern marine air masses



passing along with the coastal region had the lowest BC_{bb} fraction (35 %).

Potential sources of BC_{fr} and BC_{bb} in Xiamen with their contributions were characterized with PSCF and CWT analyses and the results are presented in Fig. 6. According to the PSCF and CWT maps of BC_{fr} (Fig. 6a, c), the strong potential sources probabilities for BC_{fr} distributed to southwest of Xiamen, including southwest Fujian province as well as Guangdong province. Significant potential sources were also located in Hubei, Anhui, Jiangxi and Henan provinces in east-central China and Hebei and Shandong provinces in north China, again implying the influences of long-range transport on BC_{fr} in Xiamen. Southeast Asia with strong regional BC emissions (Permadi et al., 2018) was also indicated as the potential source regions. For BC_{bb} , similar to BC_{fr} , the PSCF and CWT distributions (Fig. 6b, d) show that the exogenous potential sources were mainly distributed in east-central China, which belonged to the major areas of biomass burning in China (Yan et al., 2006; Huang et al., 2012; Wu et al., 2018). Guangdong province in south China was also suggested as the source of BC_{bb} . Unlike BC_{fr} , the strong potential sources probabilities from Southeast Asia to BC_{bb} were less significant.

Fig. 7 and Fig. 8 depict the seasonal PSCF and CWT distributions for BC_{fr} and BC_{bb} . Source distributions of both BC_{fr} and BC_{bb} in different seasons significantly varied due to the variability in the airflows. In spring, the terrestrial contributions from Guangdong province and north China as well as the potential source from the East China Sea for BC_{fr} and BC_{bb} were significant. The South China Sea were the main potential source for BC_{fr} and BC_{bb} during summer. In addition, high PSCF and CWT values for summer BC_{bb} were also found in north China. In fall season, similar to spring, high PSCF and CWT values for BC_{fr} and BC_{bb} were distributed in east-central China and the East China Sea. In winter, the main potential sources for BC_{fr} and BC_{bb} were also located in east-central China, while the contributions from the seas were small. The potential sources for BC_{bb} in central China were much stronger in winter than that in other seasons.

3.3 Source-oriented modeling-based source apportionment of BC

Relative source contributions to BC in Xiamen from different source sectors and fuel catalogs were assessed with the source-oriented CMAQ-PPM model. Fig. 9 illustrates the seasonal and annual average contributions of each source sector in Xiamen. Overall, transportation, residential and open burning sectors were the major sources of BC, with the annual contributions of 45.3 %, 30.1 % and 17.6 %, respectively. By comparison, power plants and industrial sectors made insignificant contributions to BC. The transportation sector was the dominant source in all seasons, especially in summer, contributing 36.5 % – 56.6 % to total BC. The residential sector contributing 20.5 % – 37.2 % was the second largest source in all seasons except spring. On contrary, power plants and industrial sectors were minor sources in all seasons, with the seasonal contributions of 2.2 % – 6.2 % and 2.8 % – 4.6 %, respectively. Obvious seasonal pattern of contribution of open burning was found. In spring and summer, open burning played a vital role by contributing 35.5 % and 17.8 %, respectively. However, its relative contributions dramatically decreased to 7.6 % in fall and 7.5 % in winter. Source contributions of the



five sectors to BC in different periods are depicted in Fig. S3. The remarkable seasonal and spatial variations from open burning are consistent with those derived in previous study (Hu et al., 2015). In spring, strong open burning in south China might significantly influence BC concentrations in the surrounding regions near the sources, which would contribute to larger biomass burning contribution in Xiamen. Intensive open burning in South Asia and Southeast Asia countries in spring
330 also affected biomass burning contribution in Xiamen through long-range transport.

Seasonal variations in simulated relative contributions of three fuel catalogs, including coal, liquid fossil fuel and biomass, to BC in Xiamen were also characterized and compared with relative contributions of biomass burning estimated according to light-absorption properties (Fig. 10). The source-oriented model almost captured the seasonal trends in contributions of fossil fuel combustion and biomass burning, although its largest seasonal contribution of biomass burning occurred in spring rather
335 than winter. For the source-oriented modeling results, liquid fossil fuel combustion had the largest contribution (46.5 %), followed by biomass burning (32.6 %) and coal combustion (20.9 %). Contributions of different fuel catalogs exhibited distinct seasonality. Seasonal contributions of coal combustion were in the order of winter (27.8 %) > fall (23.4 %) > spring (15.6 %) > summer (14.5 %). Different from coal combustion and biomass burning, liquid fossil fuel combustion had the largest contribution in summer (57.5 %) while smallest contribution (37.4 %) in spring.

340 Compared to observation-based results, relative contribution of biomass burning derived by the source-oriented modeling was 14.3 % smaller in winter, while 15.9 % larger in spring. The large gap in spring may be resulted from the uncertainties in satellite-based inventory of biomass-burning emissions in South Asia and south China (Wiedinmyer et al., 2011), while the disagreement in winter may ascribe to the underestimation of biomass-burning emissions in north and central China (Huang et al., 2012; Zhou et al., 2016). In China, some open burning activities such as local/small-scale open burning and
345 smoldering are important sources of biomass-burning BC, which was particularly the case in winter. However, these burning activities are difficult to be detected by satellite, leading to underestimation of biomass-burning emissions. The discrepancies between the results from the two source apportionment methods were much smaller in summer (1.7 %) and fall (6.0 %). Seasonal relative contributions of biomass burning estimated by the source-oriented model were in the range of 25.7 % – 47.0 %, with an annual average of 32.6 %, which was very close to the observed results derived from the Aethalometer
350 method. The consistence of the two different source apportionment methods confirms that the source apportionment results in Xiamen from this study are reasonable and benefiting future emission-control strategies.

4 Conclusions

In this study, the observation-based light absorption and source-oriented modeling were combined to reveal the contributions of biomass burning and fossil fuel combustion to ambient BC aerosol as well as their temporal variations in a relatively clean
355 region in China. The annual average concentration of BC from fossil fuel (BC_{ff}) and biomass burning (BC_{bb}) identified by



the Aethalometer method were $2932 \pm 1444 \text{ ng m}^{-3}$ and $1340 \pm 542 \text{ ng m}^{-3}$, accounting for 66.7 % and 33.3 % of total BC, respectively. For biomass burning contribution, its highest level occurred in the evening rush hour, while the maximum seasonal value was in winter. East-northeasterly and northerly wind was more likely to result in large biomass burning contribution. Air masses from the northern inland region including north China and east-central China had larger biomass
360 burning contributions. Potential sources for BC_{ff} and BC_{bb} indicate the impact of long-range transport from north and east-central China and Southeast Asia. Overall, the source-oriented model presented a good agreement with the Aethalometer method and it was able to reproduce the observed seasonal variability of biomass burning based on light absorption. Based on the source-oriented model, the transportation, residential and open burning sectors were the larger contributors to BC compared to the power and industrial sectors. The largest contribution of liquid fossil fuel combustion to BC was identified
365 by the source-oriented model, followed by biomass burning and coal combustion. The discrepancies between the two source apportionment methods suggest emission inventory with higher spatiotemporal resolution is required in future studies to provide more accurate source apportionment results of BC in China.

Data availability. The data is available upon request from Junjun Deng (dengjunjun@tju.edu.cn).
370

Author contribution. JD and HZ designed the experiments and carried them out. JD and WZ performed the analysis of observation. HG and HZ performed the source-oriented modeling. JZ, WH, LW, XW and PF provided suggestions for data analysis. JD prepared the manuscript with contributions from all co-authors.

375 *Competing interests.* The authors declare that they have no conflict of interests.

Acknowledgments. This study was supported by National Key Research and Development Program of China (2019YFA0606801) and National Natural Science Foundation of China (21607148).

References

- 380 Andersson, A., Deng, J., Du, K., Zheng, M., Yan, C., Skold, M., and Gustafsson, O.: Regionally-varying combustion sources of the January 2013 severe haze events over Eastern China, *Environ. Sci. Technol.*, 49, 2038–2043, <https://doi.org/10.1021/es503855e>, 2015.
- Ashbaugh, L. L., Malm, W. C., and Sadeh, W. Z.: A residence time probability analysis of sulfur concentrations at Grand Canyon National Park, *Atmos. Environ.*, 19 (8), 1263–1270, [https://doi.org/10.1016/0004-6981\(85\)90256-2](https://doi.org/10.1016/0004-6981(85)90256-2), 1985.
- 385 Bari, M. A., Kindzierski, W. B., Wallace, L. A., Wheeler, A. J., MacNeill, M., and Heroux, M. E.: Indoor and outdoor levels



- and sources of submicron particles (PM₁) at homes in Edmonton, Canada, *Environ. Sci. Technol.*, 49, 6419–6429, <https://doi.org/10.1021/acs.est.5b01173>, 2015.
- Bond, T. C., Doherty, S. J., Fahey, D. W., Forster, P. M., Berntsen, T., DeAngelo, B. J., Flanner, M. G., Ghan, S., Kärcher, B., Koch, D., Kinne, S., Kondo, Y., Quinn, P. K., Sarofim, M. C., Schultz, M. G., Schulz, M., Venkataraman, C., Zhang, H., Zhang, S., Bellouin, N., Guttikunda, S. K., Hopke, P. K., Jacobson, M. Z., Kaiser, J. W., Klimont, Z., Lohmann, U., Schwarz, J. P., Shindell, D., Storelvmo, T., Warren, S. G., and Zender, C. S.: Bounding the role of black carbon in the climate system: A scientific assessment, *J. Geophys. Res.-Atmos.*, 118, 5380–5552, <https://doi.org/10.1002/jgrd.50171>, 2013.
- Cao, J., Tie, X., Xu, B., Zhao, Z., Zhu, C., Li, G., and Liu, S.: Measuring and modeling black carbon (BC) contamination in the SE Tibetan Plateau, *J. Atmos. Chem.*, 67, 45, <https://doi.org/10.1007/s10874-011-9202-5>, 2010.
- 395 Chen, B., Andersson, A., Lee, M., Kirillova, E. N., Xiao, Q., Krusa, M., Shi, M., Hu, K., Lu, Z., Streets, D. G., Du, K., and Gustafsson, O.: Source Forensics of Black Carbon Aerosols from China, *Environ. Sci. Technol.*, 47, 9102–9108, <https://doi.org/10.1021/es401599r>, 2013.
- Cheng, Y., Engling, G., He, K. B., Duan, F. K., Ma, Y. L., Du, Z. Y., Liu, J. M., Zheng, M., and Weber, R. J.: Biomass burning contribution to Beijing aerosol, *Atmos. Chem. Phys.*, 13, 7765–7781, <https://doi.org/10.5194/acp-13-7765-2013>, 400 2013.
- Colicino, E., Wilson, A., Frisardi, M. C., Prada, D., Power, M. C., Hoxha, M., Dioni, L., Spiro, A., Vokonas, P. S., Weisskopf, M. G., Schwartz, J. D., and Baccarelli, A. A.: Telomere length, long-term black carbon exposure, and cognitive function in a cohort of older men: The VA normative aging study, *Environ. Health Persp.*, 125 (1), 76–81, <https://doi.org/10.1289/EHP241>, 2017.
- 405 Deng, J., Zhang, Y., Hong, Y., Xu, L., Chen, Y., Du, W., and Chen, J.: Optical properties of PM_{2.5} and the impacts of chemical compositions in the coastal city Xiamen in China, *Sci. Total Environ.*, 557–558, 665–675, <https://doi.org/10.1016/j.scitotenv.2016.03.143>, 2016.
- Deng, J., Zhao, W., Wang, X., Wu, L., Hu, W., Ren, L., and Fu, P.: Black carbon in Xiamen, China: temporal variations, transport pathways and impacts of synoptic circulation, *Chemosphere*, 241, 125133, 410 <https://doi.org/10.1016/j.chemosphere.2019.125133>, 2020.
- Ding, A. J., Fu, C. B., Yang, X. Q., Sun, J. N., Petaja, T., Kerminen, V. M., Wang, T., Xie, Y., Herrmann, E., Zheng, L. F., Nie, W., Liu, Q., Wei, X. L., and Kumala, M.: Intense atmospheric pollution modifies weather: a case of mixed biomass burning with fossil fuel combustion pollution in eastern China, *Atmos. Chem. Phys.*, 13, 10545–10554, <https://doi.org/10.5194/acp-13-10545-2013>, 2013.
- 415 Ding, A. J., Huang, X., Nie, W., Sun, J. N., Kerminen, V. M., Petaja, T., Su, H., Cheng, Y. F., Yang, X. Q., Wang, M. H., Chi, X. G., Wang, J. P., Virkkula, A., Guo, W. D., Yuan, J., Wang, S. Y., Zhang, R. J., Wu, Y. F., Song, Y., Zhu, T., Zilitinkevich, S., and Kulmala, M.: Enhanced haze pollution by black carbon in megacities in China, *Geophys. Res. Lett.*, 43 (6), 2873–2879,



- <https://doi.org/10.1002/2016GL067745>, 2016.
- 420 Dumka, U. C., Kaskaoutis, D. G., Tiwari, S., Safai, P. D., Attri, S. D., Soni, V. K., Singh, N., Mihalopoulos, N.: Assessment of biomass burning and fossil fuel contribution to black carbon concentrations in Delhi during winter, *Atmos. Environ.*, 194, 93–109, <https://doi.org/10.1016/j.atmosenv.2018.09.033>, 2018.
- Fan, J., Rosenfeld, D., Yang, Y., Zhao, C., Leung, L. R., and Li, Z.: Substantial contribution of anthropogenic air pollution to catastrophic floods in Southwest China, *Geophys. Res. Lett.*, 43 (6), 2873–2879, <https://doi.org/10.1002/2015GL064479>, 2015.
- 425 Favez, O., El Haddad, I., Piot, C., Bor áve, A., Abidi, E., Marchand, N., Jaffrezo, J.-L., Besombes, J.-L., Personnaz, M.-B., Sciare, J., Wortham, H., George, C., and D'Anna, B.: Inter-comparison of source apportionment models for the estimation of wood burning aerosols during wintertime in an Alpine city (Grenoble, France), *Atmos. Chem. Phys.*, 10, 5295–5314, <https://doi.org/10.5194/acp-10-5295-2010>, 2010.
- Ganguly, D., Jayaraman, A., Gadhavi, H., and Rajesh, T. A.: Features in wavelength dependence of aerosol absorption
430 observed over central India, *Geophys. Res. Lett.*, 32, L13821, <https://doi.org/10.1029/2005GL023023>, 2005.
- Guo, H., Kota, S. H., Sahu, S. K., Hu, J., Ying, Q., Gao, A., and Zhang, H.: Source apportionment of PM_{2.5} in North India using source-oriented air quality models, *Environ. Pollut.*, 231, 426–436, <https://doi.org/10.1016/j.envpol.2017.08.016>, 2017.
- Gustafsson, O., Krusa, M., Zencak, Z., Sheesley, R. J., Granat, L., Engstrom, E., Praveen, P. S., Rao, P. S. P., Leck, C., and Rodhe, H.: Brown Clouds over South Asia: Biomass or Fossil Fuel Combustion? *Science*, 323 (5913), 495–498,
435 <http://doi.org/10.1126/science.1164857>, 2009
- Hansen, A. D. A., Rosen, H., and Novakov, T.: The aethalometer — An instrument for the real-time measurements of optical absorption by aerosol particles, *Sci. Total Environ.*, 36, 191–196, [https://doi.org/10.1016/0048-9697\(84\)90265-1](https://doi.org/10.1016/0048-9697(84)90265-1), 1984.
- He, M., Zheng, J., Yin, S., and Zhang, Y.: Trends, temporal and spatial characteristics, and uncertainties in biomass burning emissions in the Pearl River Delta, China, *Atmos. Environ.*, 45 (24), 4051–4059,
440 <https://doi.org/10.1016/j.atmosenv.2011.04.016>, 2011.
- Helin, A., Niemi, J. V., Virkkula, A., Pirjola, L., Teinila, K., Backman, J., Aurela, M., Saarikoski, S., Ronkko, T., Asmi, E., and Timonen, H.: Characteristics and source apportionment of black carbon in the Helsinki metropolitan area, Finland, *Atmos. Environ.*, 190, 87–98, <https://doi.org/10.1016/j.atmosenv.2018.07.022>, 2018.
- Hopke, P. K., Barrie, L. A., Li, S. M., Cheng, M. D., Li, C., and Xie, Y.: Possible sources and preferred pathways for
445 biogenic and non-sea salt sulfur for the high Arctic, *J. Geophys. Res.-Atmos.*, 100 (D8), 16595–16603, <https://doi.org/10.1029/95JD01712>, 1995.
- Hsu, Y. K., Holsen, T. M., and Hopke, P. K.: Comparison of hybrid receptor models to locate PCB sources in Chicago, *Atmos. Environ.*, 37, 545–562, [https://doi.org/10.1016/S1352-2310\(02\)00886-5](https://doi.org/10.1016/S1352-2310(02)00886-5), 2003.
- Hu, J., Wu, L., Zheng, B., Zhang, Q., He, K., Chang, Q., Li, X., Yang, F., Ying, Q., and Zhang, H.: Source contributions and



- 450 regional transport of primary particulate matter in China, *Environ. Pollut.*, 207, 31–42,
<https://doi.org/10.1016/j.envpol.2015.08.037>, 2015.
- Huang, X., Li, M., Li, J., and Song, Y.: A high-resolution emission inventory of crop burning in fields in China based on MODIS Thermal anomalies/fire products, *Atmos. Environ.*, 50, 9–15, <https://doi.org/10.1016/j.atmosenv.2012.01.017>, 2012.
- Huang, X., Ding, A., Liu, L., Liu, Q., Ding, K., Niu, X., Nie, W., Xu, Z., Chi, X., Wang, M., Sun, J., Guo, W., and Fu, C.:
455 Effects of aerosol–radiation interaction on precipitation during biomass-burning season in East China, *Atmos. Chem. Phys.*,
16, 10063–10082, <https://doi.org/10.5194/acp-16-10063-2016>, 2016.
- Jacobson, M. Z.: Control of fossil-fuel particulate black carbon and organic matter, possibly the most effective method of slowing global warming, *J. Geophys. Res.-Atmos.*, 107 (D19), 4410–4431, <https://doi.org/10.1029/2001JD001376>, 2002.
- Janssen, N. A., Hoek, G., Simic-Lawson, M., Fischer, P., van Bree, L., ten Brink, H., Keuken, M., Atkinson, R. W., Anderson,
460 H. R., Brunekreef, B., and Casses, F. R.: Black Carbon as an Additional Indicator of the Adverse Health Effects of Airborne
Particles Compared with PM10 and PM2.5, *Environ. Health Persp.*, 119 (12), 1691–1699,
<https://doi.org/10.1289/ehp.1003369>, 2011.
- Jing, A., Zhu, B., Wang, H., Yu, X., An, J., and Kang, H.: Source apportionment of black carbon in different seasons in the northern suburb of Nanjing, China, *Atmos. Environ.*, 201, 190–200, <https://doi.org/10.1016/j.atmosenv.2018.12.060>, 2019.
- 465 Kalogridis, A.-C., Vratolis, S., Liakakou, E., Gerasopoulos, E., Mihalopoulos, N., and Eleftheriadis, K.: Assessment of wood
burning versus fossil fuel contribution to wintertime black carbon and carbon monoxide concentrations in Athens, Greece,
Atmos. Chem. Phys., 18, 10219–10236, <https://doi.org/10.5194/acp-18-10219-2018>, 2018.
- Kant, Y., Shaik, D. S., Mitra, D., Chandola, H. C., Babu, S. S., and Chauhan, P.: Black carbon aerosol quantification over
north-west Himalayas: Seasonal heterogeneity, source apportionment and radiative forcing, *Environ. Pollut.*, 257, 113446,
470 <https://doi.org/10.1016/j.envpol.2019.113446>, 2020
- Kim, H., Kang, S. M., Hwang, Y. T., and Yang, Y. M.: Sensitivity of the Climate Response to the Altitude of Black Carbon in
the Northern Subtropics in an Aquaplanet GCM, *J. Climate*, 16, 6351–6359, <https://doi.org/10.1175/JCLI-D-15-0037.1>,
2015.
- Kirchstetter, T. W., Novakov, T., and Hobbs, P. V.: Evidence that the spectral dependence of light absorption by aerosols is
475 affected by organic carbon, *J. Geophys. Res.-Atmos.*, 109, D21208, <http://doi.org/10.1029/2004JD004999>, 2004.
- Kleeman, M.J., Ying, Q., Lu, J., Mysliwiec, M.J., Griffin, R.J., Chen, J.J., and Clegg, S.: Source apportionment of secondary
organic aerosol during a severe photochemical smog episode, *Atmos. Environ.*, 41 (3), 576–591,
<https://doi.org/10.1016/j.atmosenv.2006.08.042>, 2007.
- Kurokawa, J., Ohara, T., Morikawa, T., Hanayama, S., Janssens-Maenhout, G., Fukui, T., Kawashima, K., and Akimoto, H.:
480 Emissions of air pollutants and greenhouse gases over Asian regions during 2000–2008: Regional Emission inventory in
ASia (REAS) version 2, *Atmos. Chem. Phys.*, 13, 11019–11058, <https://doi.org/10.5194/acp-13-11019-2013>, 2013.



- Li, K., Liao, H., Mao, Y., and Ridley, D. A.: Source sector and region contributions to concentration and direct radiative forcing of black carbon in China, *Atmos. Environ.*, 124, 351–366, <https://doi.org/10.1016/j.atmosenv.2015.06.014>, 2016.
- Li, N., He, Q., Tie, X., Cao, J., Liu, S., Wang, Q., Li, G., Huang, R., and Zhang, Q.: Quantifying sources of elemental carbon over the Guanzhong Basin of China: A consistent network of measurements and WRF-Chem modeling, *Environ. Pollut.*, 214, 86–93, <https://doi.org/10.1016/j.envpol.2016.03.046>, 2016.
- Liu, D., Allan, J. D., Young, D. E., Coe, H., Beddows, D., Fleming, Z. L., Flynn, M. J., Gallagher, M. W., Harrison, R. M., Lee, J., Prevot, A. S. H., Taylor, J. W., Yin, J., Williams, P. I., and Zotter, P.: Size distribution, mixing state and source apportionment of black carbon aerosol in London during wintertime, *Atmos. Chem. Phys.*, 14, 10061–10084, <https://doi.org/10.5194/acp-14-10061-2014>, 2014.
- Lou, S., Yang, Y., Wang, H., Smith, S. J., Qian, Y., and Rasch, P. J.: Black Carbon Amplifies Haze Over the North China Plain by Weakening the East Asian Winter Monsoon, *Geophys. Res. Lett.*, 46 (1), 452–460, <https://doi.org/10.1029/2018GL080941>, 2019.
- Martinsson, J., Abdul Azeem, H., Sporre, M. K., Bergström, R., Ahlberg, E., Öström, E., Kristensson, A., Swietlicki, E., and Eriksson Stenström, K.: Carbonaceous aerosol source apportionment using the Aethalometer model – evaluation by radiocarbon and levoglucosan analysis at a rural background site in southern Sweden, *Atmos. Chem. Phys.*, 17, 4265–4281, <https://doi.org/10.5194/acp-17-4265-2017>, 2017.
- Mbengue, S., Serfozo, N., Schwarz, J., Zikova, N., Smejkalova, A. H., and Holoubek, I.: Characterization of Equivalent Black Carbon at a regional background site in Central Europe: Variability and source apportionment, *Environ. Pollut.*, 260, 113771, <https://doi.org/10.1016/j.envpol.2019.113771>, 2020.
- Menon, S., Hansen, J., Nazarenko, L., and Luo, Y.: Climate effects of black carbon aerosols in China and India, *Science*, 297 (5590), 2250–2253, <https://doi.org/10.1126/science.1075159>, 2002.
- Mousavi, A., Sowlat, M. H., Hasheminassab, S., Polidori, A., and Sioutas, C.: Spatio-temporal trends and source apportionment of fossil fuel and biomass burning black carbon (BC) in the Los Angeles Basin, *Sci. Total Environ.*, 640–641, 1231–1240, <https://doi.org/10.1016/j.scitotenv.2018.06.022>, 2018.
- Mousavi, A., Sowlat, M. H., Lovett, C., Rauber, M., Szidat, S., Boffi, R., Borgini, A., Marco, C. D., Ruprecht, A. A., and Sioutas, C.: Source apportionment of black carbon (BC) from fossil fuel and biomass burning in metropolitan Milan, Italy, *Atmos. Environ.*, 203, 252–261, <https://doi.org/10.1016/j.atmosenv.2019.02.009>, 2019.
- Peng, J., Hu, M., Guo, S., Du, Z., Zheng, J., Shang, D., Zamora, M. L., Zeng, L., Shao, M., Wu, Y. S., Zheng, J., Wang, Y., Glen, C. R., Collins, D. R., Molina, M. J., and Zhang, R.: Markedly enhanced absorption and direct radiative forcing of black carbon under polluted urban environments, *P. Natl. Acad. Sci. USA*, 113 (16), 4266–4271, <https://doi.org/10.1073/pnas.1602310113>, 2016.
- Permadi, D. A., Kim Oanh, N. T., and Vautard, R.: Integrated emission inventory and modeling to assess distribution of



- particulate matter mass and black carbon composition in Southeast Asia, *Atmos. Chem. Phys.*, 18, 2725–2747,
515 <https://doi.org/10.5194/acp-18-2725-2018>, 2018.
- Qian, Y., Wang, H., Zhang, R., Flanner, M. G., and Rasch, P. J.: A sensitivity study on modeling black carbon in snow and its radiative forcing over the Arctic and Northern China, *Environ. Res. Lett.*, 9 (6), 064001, <https://doi.org/10.1088/1748-9326/9/6/064001>, 2014.
- Qiu, Y., Wu, X., Zhang, Y., Xu, L., Hong Y., Chen, J., Chen, X., and Deng, J.: Aerosol light absorption in a coastal city in
520 Southeast China: temporal variations and implications for brown carbon, *J. Environ. Sci.*, 80, 257–266, <https://doi.org/10.1016/j.jes.2019.01.002>, 2019.
- Rajesh, T. A., and Ramachandran, S.: Characteristics and source apportionment of black carbon aerosols over an urban site, *Environ. Sci. Pollu. Res.*, 24, 8411–8424, <https://doi.org/10.1007/s11356-017-8453-3>, 2017.
- Ramanathan, V., and Carmichael, G.: Global and regional climate changes due to black carbon, *Nat. Geosci.*, 1, 221–227,
525 <https://doi.org/10.1038/ngeo156>, 2008.
- Rehman, I. H., Ahmed, T., Praveen, P. S., Kar, A., and Ramanathan, V.: Black carbon emissions from biomass and fossil fuels in rural India, *Atmos. Chem. Phys.*, 11, 7289–7299, <https://doi.org/10.5194/acp-11-7289-2011>, 2011.
- Saide, P. E., Spak, S. N., Pierce, R. B., Otkin, J. A., Schaack, T. K., Heidinger, A. K., daSilva, A. M., Kacenenbogen, M., Redemann, J., and Carmichael, G. R.: Central American biomass burning smoke can increase tornado severity in the U.S.,
530 *Geophys. Res. Lett.*, 42, 956–965, <https://doi.org/10.1002/2014GL062826>, 2015.
- Sandradewi, J., Prevot, A. S. H., Szidat, S., Perron, N., Alfarra, M. R., Lanz, V. A., Weingartner, E., and Baltensperger, U.: Using aerosol light absorption measurements for the quantitative determination of wood burning and traffic emission contributions to particulate matter, *Environ. Sci. Technol.*, 42 (9), 3316–3323, <https://doi.org/10.1021/es702253m>, 2008.
- Stein, A. F., Draxler, R. R., Rolph, G. D., Stunder, B. J. B., Cohen, M. D., and Ngan, F.: NOAA's HYSPLIT atmospheric transport and dispersion modeling system, *B. Am. Meteorol. Soc.*, 96, 2059–2077, <https://doi.org/10.1175/BAMS-D-14-00110.1>, 2015.
- Vaishya, A., Singh, P., Rastogi, S., and Babu, S. S.: Aerosol black carbon quantification in the central Indo-Gangetic Plain: Seasonal heterogeneity and source apportionment, *Atmos. Res.*, 185, 13–21, <https://doi.org/10.1016/j.atmosres.2016.10.001>, 2017.
- 540 Venkataraman, C., Habib, G., Eiguren-Fernandez, A., Miguel, A. H., and Friedlander, S. K.: Residential biofuels in south Asia: carbonaceous aerosol emissions and climate impacts, *Science*, 307, 1454–1456, <https://doi.org/10.1126/science.1104359>, 2005.
- Virkkula, A., Mäkelä T., Hillamo, R., Yli-Tuomi, T., Hirsikko, A., Hämeri, K., and Koponen, I. K.: A simple procedure for correcting loading effects of Aethalometer data, *J. Air Waste Manage.*, 57, 10, 1214–1222,
545 <https://doi.org/10.3155/1047-3289.57.10.1214>, 2007.



- Wang, Q. Y., Huang, R.-J., Cao, J. J., Tie, X. X., Ni, H. Y., Zhou, Y. Q., Han, Y. M., Hu, T. F., Zhu, C. S., Feng, T., Li, N., and Li, J. D.: Black carbon aerosol in winter northeastern Qinghai–Tibetan Plateau, China: the source, mixing state and optical property, *Atmos. Chem. Phys.*, 15, 13059–13069, <https://doi.org/10.5194/acp-15-13059-2015>, 2015.
- Wang, R., Tao, S., Wang, W., Liu, J., Shen, H., Shen, G., Wang, B., Liu, X., Li, W., Huang, Y., Zhang, Y., Lu, Y., Chen, H.,
550 Chen, Y., Wang, C., Zhu, D., Wang, X., Li, B., Liu, W., and Ma, J.: Black carbon emissions in China from 1949 to 2050, *Environ. Sci. Technol.*, 46, 7595–7603, <https://doi.org/10.1021/es3003684>, 2012.
- Wang, Z., Huang, X., and Ding, A.: Dome effect of black carbon and its key influencing factors: a one-dimensional modelling study, *Atmos. Chem. Phys.*, 18, 2821–2834, <https://doi.org/10.5194/acp-18-2821-2018>, 2018.
- Watson, J. G.: Visibility: science and regulation, *J. Air Waste Manage.*, 52, 628–713,
555 <https://doi.org/10.1080/10473289.2002.10470813>, 2002.
- Wiedinmyer, C., Akagi, S. K., Yokelson, R. J., Emmons, L. K., Al-Saadi, J. A., Orlando, J. J., and Soja, A. J.: The Fire INventory from NCAR (FINN): a high resolution global model to estimate the emissions from open burning, *Geosci. Model Dev.*, 4, 625–641, <https://doi.org/10.5194/gmd-4-625-2011>, 2011.
- Winiger, P., Barrett, T. E., Sheesley, R. J., Huang, L., Sharma, S., Barrie, L. A., Yttri, K. E., Evangeliou, N., Eckhardt, S.,
560 Stohl, A., Klimont, Z., Heyes, C., Semiletov, I. P., Dudarev, O. V., Charkin, A., Shakhova, N., Holmstrand, H., Andersson, A., and Gustafsson, O.: Source apportionment of circum-Arctic atmospheric black carbon from isotopes and modeling, *Sci. Adv.*, 5, eaau8052, <https://doi.org/10.1126/sciadv.aau8052>, 2019.
- Wu, D., Wu, C., Liao, B., Chen, H., Wu, M., Li, F., Tan, H., Deng, T., Li, H., Jiang, D., and Yu, J. Z.: Black carbon over the South China Sea and in various continental locations in South China, *Atmos. Chem. Phys.*, 13, 12257–12270,
565 <https://doi.org/10.5194/acp-13-12257-2013>, 2013.
- Wu, J., Kong, S., Wu, F., Cheng, Y., Zheng, S., Yan, Q., Zheng, H., Yang, G., Zheng, M., Liu, D., Zhao, D., and Qi, S., 2018: Estimating the open biomass burning emissions in central and eastern China from 2003 to 2015 based on satellite observation, *Atmos. Chem. Phys.*, 18, 11623–11646.
- Yan, X., Ohara, T., and Akimoto, H.: Bottom-up estimate of biomass burning in mainland China, *Atmos. Environ.*, 40 (27),
570 5262–5273, <https://doi.org/10.1016/j.atmosenv.2006.04.040>, 2006.
- Yang, Y., Wang, H., Smith, S.J., Ma, P.L., and Rasch, P.J.: Source attribution of black carbon and its direct radiative forcing in China, *Atmos. Chem. Phys.*, 17, 4319–4336, <https://doi.org/10.5194/acp-17-4319-2017>, 2017.
- Ying, Q., Lu, J., Kaduwela, A., and Kleeman, M.: Modeling air quality during the California REGIONAL PM₁₀/PM_{2.5} Air Quality Study (CPRAQS) using the UCD/CIT Source Oriented Air Quality Model - Part II. Regional source apportionment
575 of primary airborne particulate matter, *Atmos. Environ.*, 42 (39), 8967–8978, <https://doi.org/10.1016/j.atmosenv.2008.05.065>, 2008.
- Yu, K., Xing, Z., Huang, X., Deng, J., Andersson, A., Fang, W., Gustafsson, O., Zhou, J., and Du, K.: Characterizing and



- sourcing ambient PM_{2.5} over key emission regions in China III: Carbon isotope based source apportionment of black carbon, *Atmos. Environ.*, 177, 12–17, <https://doi.org/10.1016/j.atmosenv.2018.01.009>, 2018.
- 580 Zhang, H., DeNero, S.P., Joe, D.K., Lee, H.H., Chen, S.H., Michalakes, J., and Kleeman, M.J.: Development of a source oriented version of the WRF/Chem model and its application to the California regional PM₁₀/PM_{2.5} air quality study, *Atmos. Chem. Phys.*, 14 (1), 485–503, <https://doi.org/10.5194/acp-14-485-2014>, 2014.
- Zhang, Y., Zhang, H., Deng, J., Du, W., Hong, Y., Xu, L., Qiu, Y., Hong, Z., Wu, X., Ma, Q., and Yao, J.: Source regions and transport pathways of PM_{2.5} at a regional background site in East China, *Atmos. Environ.*, 167, 202–211, 585 <https://doi.org/10.1016/j.atmosenv.2017.08.031>, 2017.
- Zhang, Y., Li, M., Cheng, Y., Geng, G., Hong, C., Li, H., Li, X., Tong, D., Wu, N., Zhang, X., Zheng, B., Zheng, Y., Bo, Y., Su, H., and Zhang, Q.: Modeling the aging process of black carbon during atmospheric transport using a new approach: a case study in Beijing, *Atmos. Chem. Phys.*, 19, 9663–9680, <https://doi.org/10.5194/acp-19-9663-2019>, 2019.
- Zheng, H., Kong, S., Wu, F., Cheng, Y., Niu, Z., Zheng, S., Yang, G., Yao, L., Yan, Q., Wu, J., Zheng, M., Chen, N., Xu, K., 590 Yan, Y., Liu, D., Zhao, D., Zhao, T., Bai, Y., Li, S., and Qi, S.: Intra-regional transport of black carbon between the south edge of the North China Plain and central China during winter haze episodes, *Atmos. Chem. Phys.*, 19, 4499–4516, <https://doi.org/10.5194/acp-19-4499-2019>, 2019.
- Zhou, Y., Xing, X., Lang, J., Chen, D., Cheng, S., Wei, L., Wei, X., and Liu, C.: A comprehensive biomass burning emission inventory with high spatial and temporal resolution in China, *Atmos. Chem. Phys.*, 17, 2839–2864, 595 <https://doi.org/10.5194/acp-17-2839-2017>, 2017.
- Zotter, P., Herich, H., Gysel, M., El-Haddad, I., Zhang, Y., Mocnik, G., Hüglin, C., Baltensperger, U., Szidat, S., and Prevot, A. S. H.: Evaluation of the absorption Ångström exponents for traffic and wood burning in the Aethalometer-based source apportionment using radiocarbon measurements of ambient aerosol, *Atmos. Chem. Phys.*, 17, 4229–4249, <https://doi.org/10.5194/acp-17-4229-2017>, 2017.

600

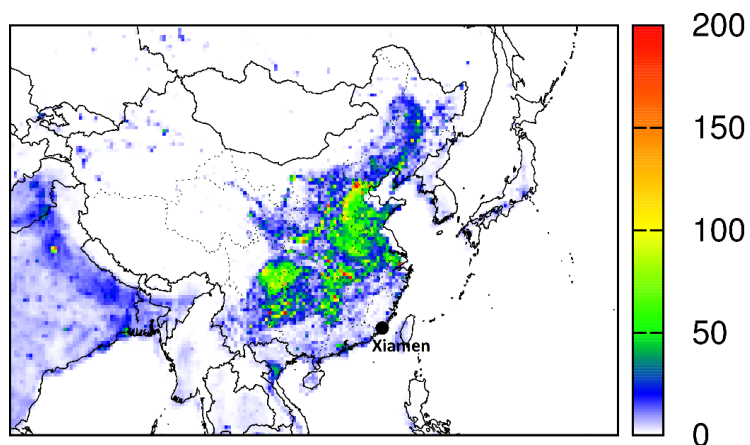
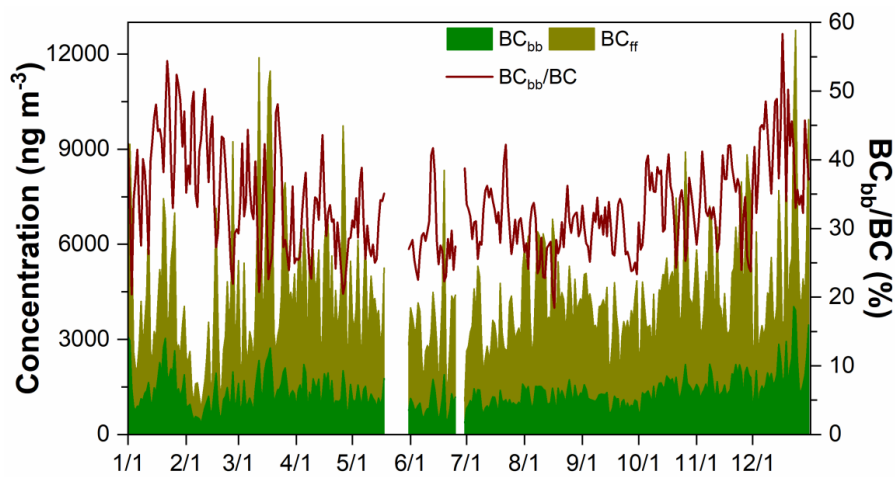


Figure 1. Location of Xiamen, China, with spatial distribution of annual average BC emission rate (g s^{-1}). BC emission data in China are from the MEIC inventory developed by Tsinghua University.



605

Figure 2. Daily BC_{ff} and BC_{bb} concentrations and $\text{BC}_{\text{bb}}/\text{BC}$ fraction in Xiamen in 2014.

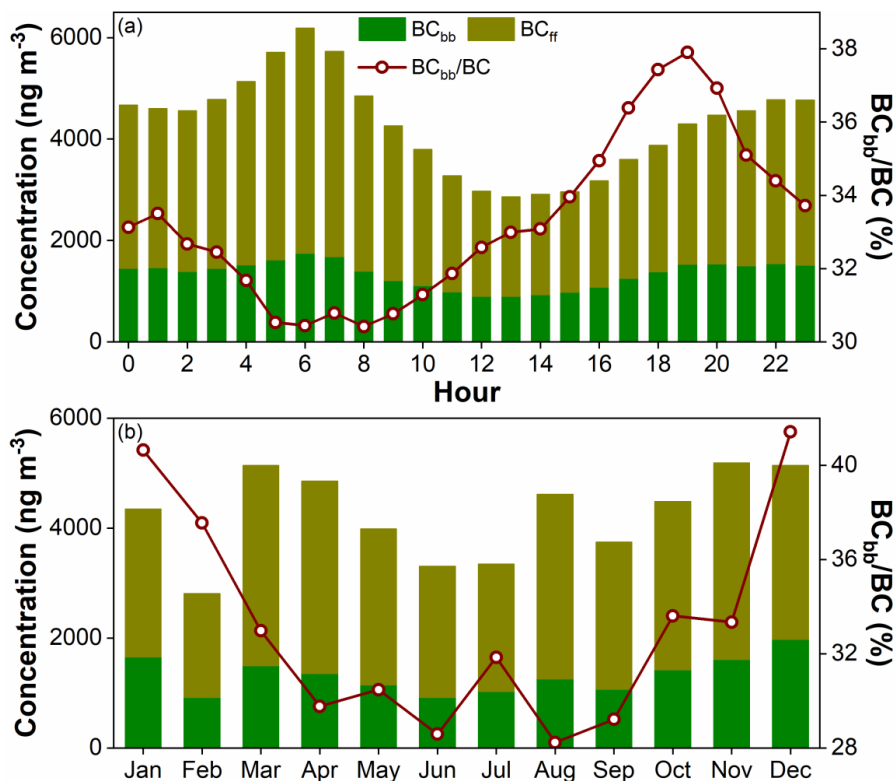


Figure 3. Diurnal and monthly variations in BC_{fr} and BC_{bb} concentrations with the BC_{bb}/BC fraction.

610

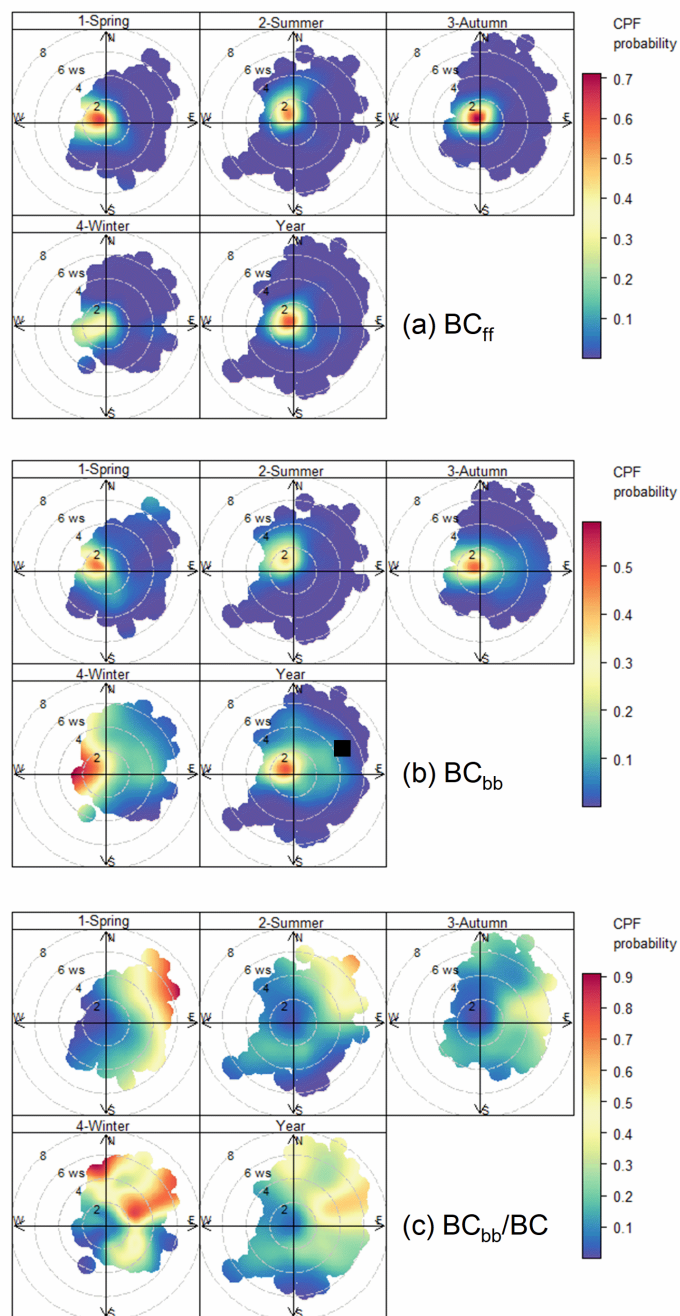
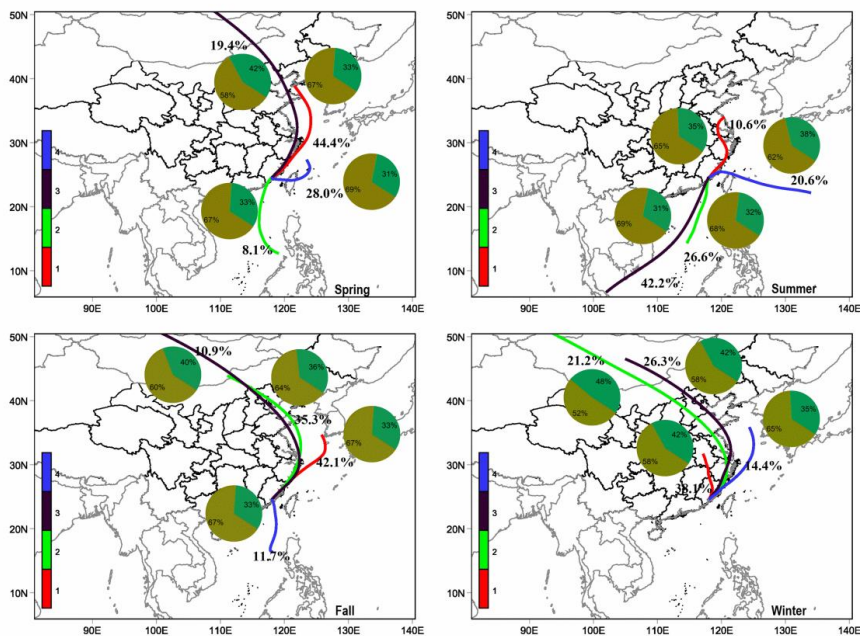
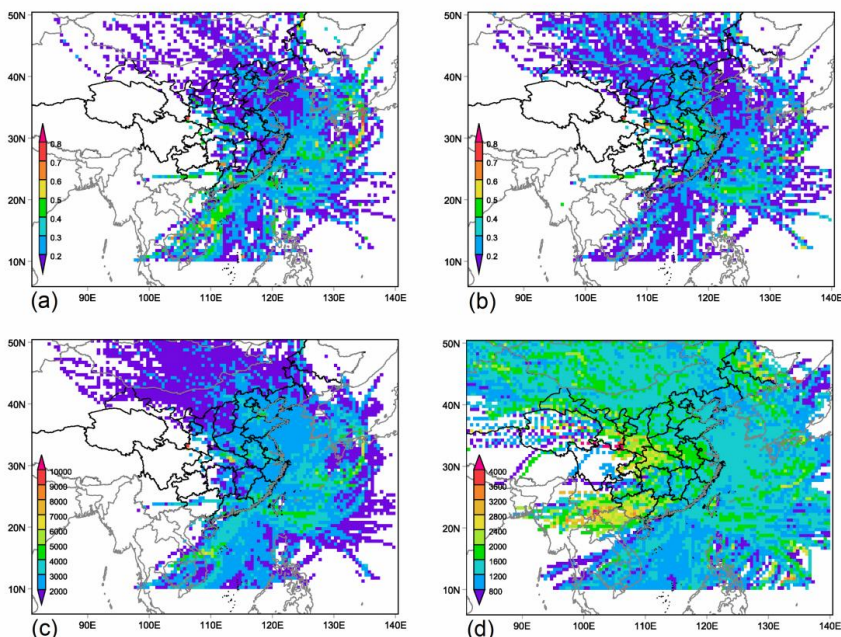


Figure 4. CPF plots for (a) BC_{ff} , (b) BC_{bb} and (c) BC_{bb}/BC contribution in Xiamen in 2014. ws represents wind speed ($m\ s^{-1}$).



615 **Figure 5. Seasonal cluster-mean of five-day backward trajectories at 500 m with the corresponding trajectory percentages and BC_{bb} contributions in Xiamen.**



620 **Figure 6. Potential source contribution function (PSCF) maps for (a) BC_{ff} and (b) BC_{bb} and concentration-weighted trajectory (CWT) maps ($ng\ m^{-3}$) for (c) BC_{ff} and (d) BC_{bb} in Xiamen in 2014.**

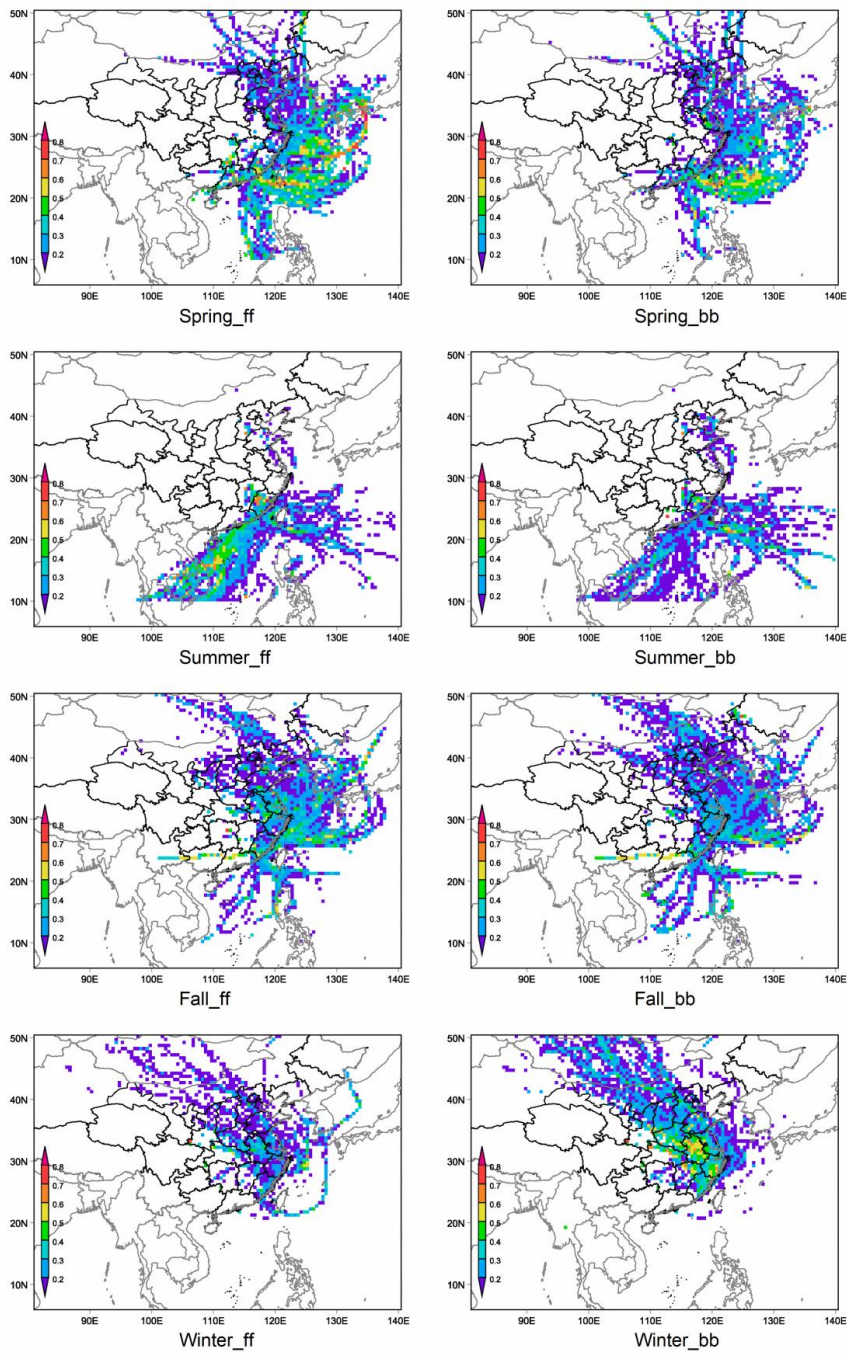
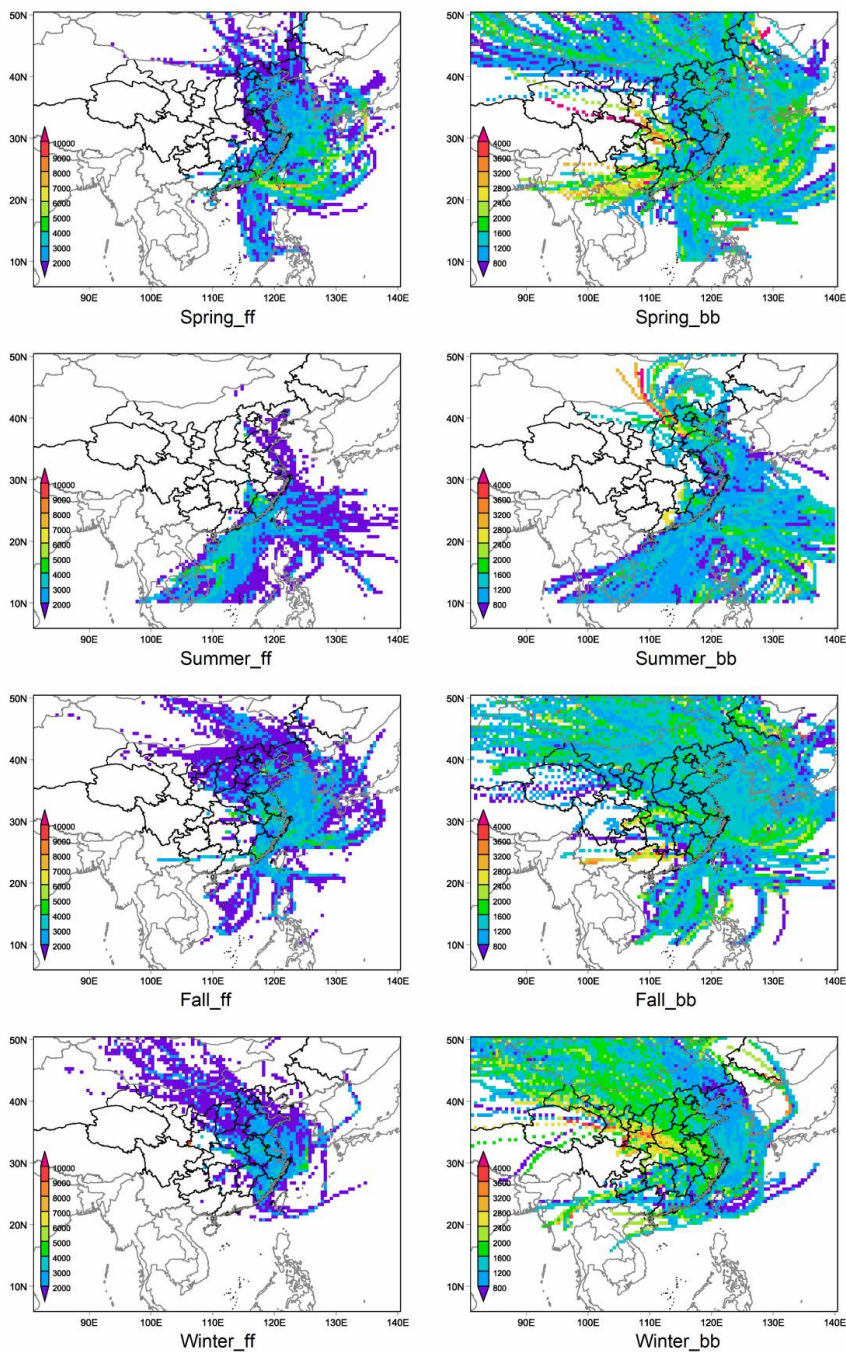


Figure 7. Potential source contribution function (PSCF) maps for BC_{ff} and BC_{bb} in Xiamen for different seasons in 2014.



625

Figure 8. Concentration weighted trajectory (CWT) maps for BC_f and BC_b in Xiamen for different seasons in 2014.

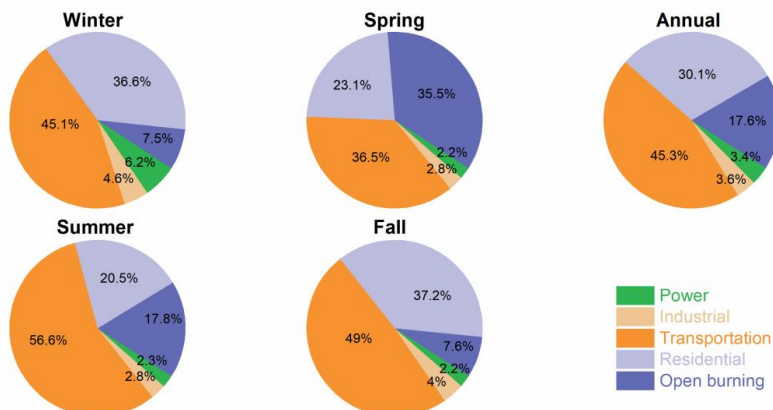


Figure 9. Source contributions to BC of five source sectors in each period.

630

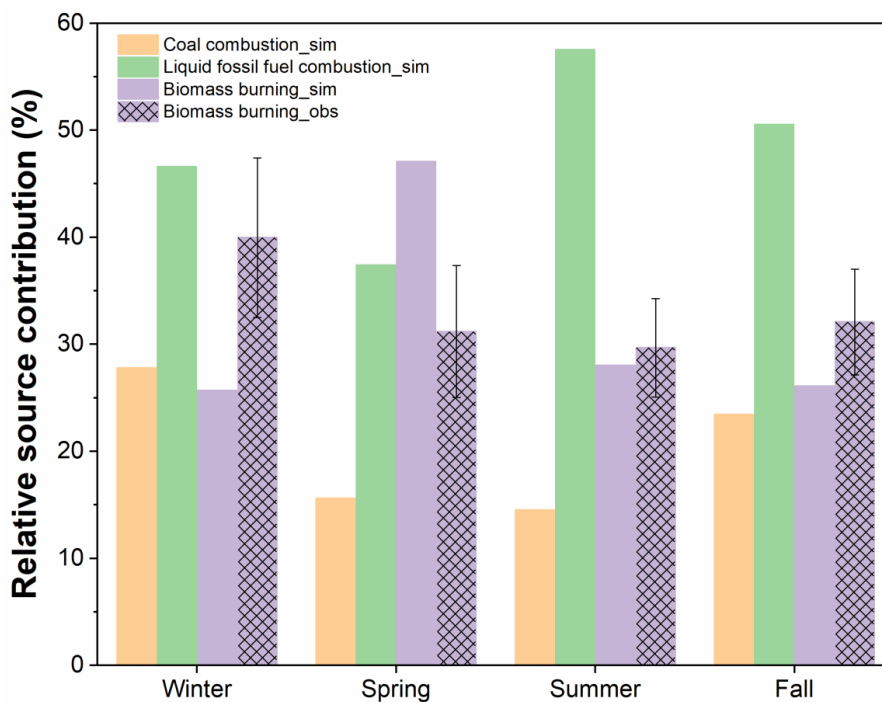


Figure 10. (a) Seasonal and (b) diurnal variations in relative source contribution of three fuel catalogs to BC in Xiamen.